Late Pleistocene-Holocene volcanic activity in northern Victoria Land recorded in Ross Sea (Antarctica) marine sediments

P. Del Carlo[1] · **A. Di Roberto**[1] · **G. Di Vincenzo**[2] · **A. Bertagnini**[1] · **P. Landi**[1] · **M. Pompilio**[1] · **E. Colizza**[3] · **G. Giordano**[4]

Accepted: 28 March 2015

Abstract Eight pyroclastic fall deposits have been identified in cores of Late Pleistocene-Holocene marine sediments from the Ross Sea (Antarctica), and their components, granulometry and clast morphologies were analysed. Sedimentological, petrographic and geochemical analysis of clasts, with ^{40}Ar-^{39}Ar dating of alkali feldspar grains, indicate that during this period at least five explosive eruptions of mid to high intensity (plinian to subplinian) occurred, and that three of these eruptions took place from Mount Melbourne volcanic complex, between 137.1 ± 3.4 and 12 ka. Geochemical comparison of the studied tephra with micro- and crypto-tephra recovered from deep Antarctic ice cores and from nearby englacial tephra at Frontier Mountain indicates that eruptive activity in the Melbourne Volcanic Province of northern Victoria Land was intense during the Late Pleistocene-Holocene, but only a general area of provenance for the majority of the identified tephra can be identified.

✉ P. Del Carlo
delcarlo@pi.ingv.it

[1] Istituto Nazionale di Geofisica e Vulcanologia, Sezione di Pisa, Via della Faggiola 32, 56126 Pisa, Italy

[2] Istituto di Geoscienze e Georisorse, CNR, via Moruzzi 1, 56124 Pisa, Italy

[3] Dipartimento di Matematica e Geoscienze, Università di Trieste, Via E. Weiss 2, 34127 Trieste, Italy

[4] Dipartimento Scienze Geologiche, Università Roma Tre, Largo San Leonardo Murialdo 1, 00146 Rome, Italy

Keywords Antarctica · Melbourne volcanic province · Gravity cores · Marine tephra · ^{40}Ar-^{39}Ar dating

Introduction

Tephra layers are isochronous surfaces on a geological timescale. When distinctive and sufficiently widespread, they represent valuable stratigraphic tools for geological correlation and dating (Lowe 2011 and references therein). In polar regions, tephra layers have been widely used as a chronostratigraphic tool (Smellie 1999; Wilch et al. 1999; Dunbar et al. 2003; Narcisi et al. 2006; Dunbar and Kurbatov 2011; Di Roberto et al. 2012) to obtain independent age constraints for glaciological modelling (Narcisi et al. 2006; Curzio et al. 2008) and to synchronize palaeoclimatic proxies from widely spaced records (Davies et al. 2010; Narcisi et al. 2012).

Victoria Land (Antarctica, Fig. 1) has been the site of intense and recurrent volcanic activity since 150 ka (LeMasurier and Thomson 1990; Kyle 1982; Armienti and Tripodo 1991; Perchiazzi et al. 1999; Esser and Kyle 2002). This activity has produced abundant and widespread subaerial fallout deposits found in the region's outcrops and embedded in the ice sheets (Keys et al. 1977; Perchiazzi et al. 1999; Laurenzi et al. 2003; Curzio et al. 2008). Records of Late Pleistocene-Holocene subaerial volcanic activity in Victoria Land are also present in marine sediments from the Ross Sea, which contain several tephra layers. Previous studies on Ross Sea marine sediments, including radiocarbon dating, suggest that some of these tephra are primary pyroclastic fall deposits emplaced between 29 and 22 thousand ^{14}C yr B.P (Licht et al. 1999; Colizza et al. 2003). The volcanoes of the Melbourne Volcanic Province (LeMasurier and Thomson 1990) are considered the most likely sources for these tephra on the basis of volcanological, geochemical and age constraints. In particular, most tephra

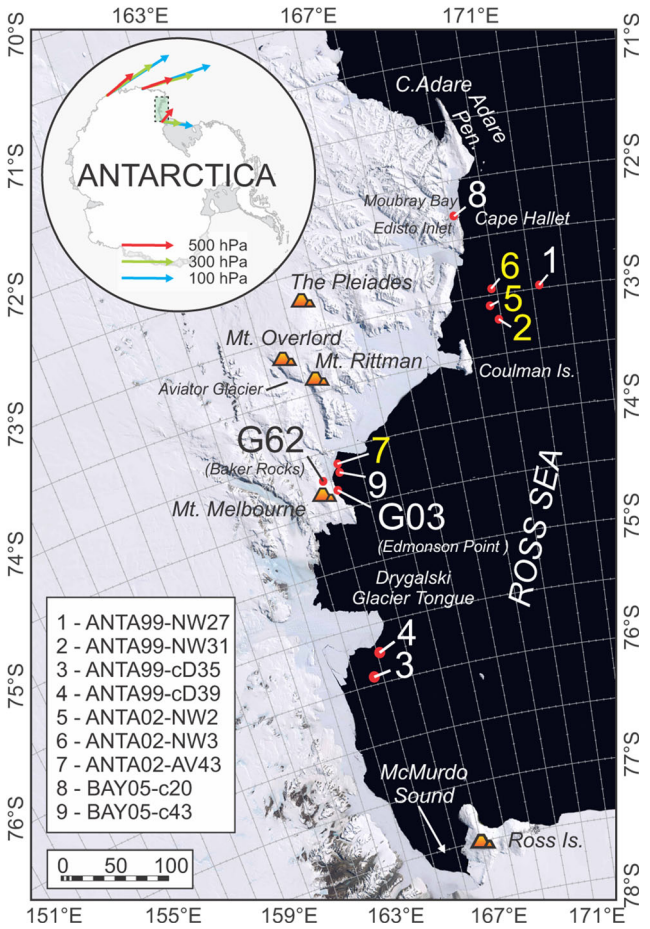

Fig. 1 Map of Victoria Land (Antarctica) showing the location of the studied cores in the Ross Sea and relevant geological features. The locations of the four cores where tephra have been identified and characterized are *highlighted in yellow*. The map also shows main volcanic complexes of the Victoria Land that were active during the Late Pleistocene-Holocene. Satellite map from Polar Geospatial Center (PGC) (ANT REF-MS2006-006). Average wind directions at 500 hPa (*red arrow*; ~5 km altitude), 300 hPa (*green arrow*; ~9 km altitude) and 100 hPa (*blue arrow*; ~12 km altitude) measured in the studied area (Connolley and King 1993) are indicated by *arrows*.

deposits are attributed to the Mount Melbourne, Mount Rittmann and the Pleiades recently active volcanoes (Fig. 1), though it has been impossible to ascribe the deposits to specific eruptions because the eruptive history of these three volcanoes is still poorly known. Giordano et al. (2012) recently characterized Pleistocene volcanic products of Mt. Melbourne using new stratigraphic data, age determinations, petrology and geochemistry. In addition, recent investigations have revealed that volcanic centres in Marie Byrd Land or beneath West Antarctic Ice Sheets might have erupted explosively in the Holocene and produced tephra layers (Behrendt 2012; Lough et al. 2013).

Given that tephra horizons are regionally better preserved in marine environments than in subaerial ones (Engwell et al. 2014), we decided to analyse in detail tephra layers in marine cores recovered during the last 30 years by Italian Antarctic Research Program (PNRA). We report here the results of tephrostratigraphic and geochemical studies on eight tephra beds identified in marine sediment sequences from Ross Sea gravity cores. Core sites are south, southeast and east of the main volcanic complexes in Victoria Land (Mount Melbourne, Mount Rittmann and The Pleiades). Moreover, we provide ^{40}Ar-^{39}Ar data on alkali feldspar crystals extracted from identified tephra beds.

Study sites

Nine gravity cores were selected from among those recovered in the Ross Sea during the 1999, 2000 and 2005 cruises (Fig. 1) and stored in the Italian repository at the Museo Nazionale dell'Antartide (Trieste, Italy). Four of the nine cores (ANTA99-NW27 and -NW31, ANTA02-NW02 and -NW03) were studied previously by Colizza et al. (2003). The nine cores are distributed along the coast of Victoria Land (Fig. 1), in an area extending from the Dryglaski Glacier Tongue to Cape Hallet. Downwind areas of the main volcanic edifices of the north Victoria Land (Mount Melbourne, Mount Rittmann and The Pleiades) were targeted for the cores selection. This on the basis of nowadays average wind directions at 500 hPa (~5.5 km altitude), 300 hPa (~9 km altitude) and 100 hPa (~12 km altitude) that for the studied area are mainly westerly (Connolley and King 1993).

Cores ANTA99-NW27 and NW31, ANTA02-NW2 and NW3 were collected north of Coulman Island in the northern Drygalski Trough at depth of 524, 535, 588 and 534 m, respectively (Fig. 1). Cores that are located in the axis of the trough that in this part of the basin are about 600 m deep. The morphology of this area is very articulated and characterized by drumlins, mega-scale glacial lineations and iceberg furrows (Shipp et al. 1999) parallel to the through axes. Cores ANTA99-cD35 and cD39 were collected south of the Drygalski Ice Tongue (inner part of Drygalsky Trough) at 886 and 845 m depth, respectively (Fig. 1). The depocentre of the basin in the inner part is more than 900 m. The sea floor morphology is complex with a draping deposit characterized by undisturbed sedimentation and lack of gravity flows. Cores ANTA02-AV43 and BAY05-c43 are located on western side of a depocentre, a >1000-m deep basin near the outlet of Aviator Glacier at a depth of 916 and 1033 m, respectively. This basin is oriented WNW-ESE and is connected to the Drygalski Basin through a morphological sill. Core BAY05-c20 was collected at the entrance of the Edisto Inlet, along the conjunction between Cape Hallett and Cape Christie. Edisto Inlet is a small bay, about 15 km long and 4 km wide, about 500 m deep and separated by a sill from the larger Moubray Bay. Core locations, recovery parameters and water depth of sampling are reported in Online Resource 1.

Materials and methods

For all nine cores, stratigraphic logging and identification of the main lithologies were carried out by visual inspection.

Sixty-four beds of unconsolidated sediments containing volcanic particles were identified and sampled for this study. All samples were washed in an ultrasonic bath for 5 minutes and subsequently wet-sieved at one φ (phi=negative log base 2 of the grain diameter) for the −3 φ (8 mm) to +5 φ (0.032 mm) grain size range. The Mdφ (mean diameter) and σφ (sorting) were calculated from the grain size distribution (Inman 1952; Table 1).

The nature, texture and qualitative abundance of components were determined using a stereomicroscope. These preliminary data were used to select volcaniclastic deposits (pyroclastic fall deposits, volcaniclastic deposits and volcanogenic sedimentary deposits according to the terminology of McPhie et al. 1993) for scanning electron microscopy and microprobe analyses. The quantitative abundance of deposit components was determined on the −3 to 0 φ (8–1 mm) grain size fractions; about 1000 clasts were counted in each sample. The selected samples were mounted with epoxy resin and prepared as standard polished thin sections.

Morphological and micro-textural analyses of components were performed using an optical microscope and a scanning electron microscope (SEM) Zeiss EVO MA 10 at Istituto Nazionale di Geofisica e Vulcanologia (Pisa). The major element composition of volcanic glass (Table 2) was determined at the HPHT Laboratory of Istituto Nazionale di Geofisica e Vulcanologia (Rome) using a JEOL JXA 8200 microprobe equipped with 5 wavelength-dispersive spectrometers (WDS) and an energy-dispersive analytical system (EDS). Instrumental conditions were 15 kV accelerating voltage, 12 nA beam current, 5 μm probe diameter, 10 and 5 s acquisition time for peak and background, respectively. A minimum of 10 points was analysed in each sample. Chemical analysis of mineral was performed at Istituto Nazionale di Geofisica e Vulcanologia (Pisa) using a Zeiss EVO MA 10 equipped with an Oxford ISIS microanalytical system on crystals 0.5–2 mm in size.

In addition, we analysed the major element composition of glass in five pyroclastic deposits sampled from the summit cone of the Mount Melbourne volcano and from Edmonson Point and Baker Rocks. These samples were collected during the XVIII Italian Expedition in 2002–2003 and may represent the proximal/medial deposits of eruptions of which distal deposits were found in the cores studied. Sample locations, ages and bulk rock compositions are reported in Giordano et al. (2012).

^{40}Ar-^{39}Ar analyses of single grains or multigrain splits of alkali feldspar were completed at IGG-CNR (Pisa), following the procedures described in Di Vincenzo and Skála (2009) and Di Vincenzo et al. (2010). Analyses were achieved using the total fusion technique and a CO_2 laser system for gas extraction. Ages are relative to the 28.34 Ma Taylor Creek sanidine (TCs; Renne et al. 1998) and were calculated using the constants recommended by Steiger and Jäger (1977). We adopted old constants due to the lack of general consensus on the ^{40}K decay constants. Note that the use of the total ^{40}K decay

Table 1 Layer thickness and main grain size parameters Mdφ and σφ for primary pyroclastic fall and slightly resedimented volcaniclastic deposits identified in the studied cores

Sample	Layer thickness (cm)	Sample depth in core (cm)	Md	σ
ANTA02-NW2-0-13	13	3.5–4.5	0.97	2.68
ANTA02-NW2-213-230	17	225–226	1.44	1.43
ANTA02-NW2-255-265	10	256–257	0.42	2.27
ANTA02-NW3-25-35	10	0–1	1.45	1.75
		11–12	0.62	2.38
		20–21	1.67	1.37
		28–29	1.42	1.64
		32.5–33.5	1.36	1.70
ANTA99-NW31-42-61	28	51–52	1.09	2.10
		54–56	−0.60	2.32
ANTA99-NW31-173-205	32	179–180	1.54	2.24
		186–187	1.59	2.12
		190–191	−0.22	2.18
		197–198	−0.71	2.17
ANTA02-AV43-137-148	11	138–139	2.40	1.57
		143–144	1.21	2.02
ANTA02-AV43-148-151	3	149–150	1.23	1.74

Table 2 Glass composition (EPMA) of tephra identified in cores and of samples from Mount Melbourne

Core	NW2						NW3		NW31				AV43				G03		G63	
cm b.s.f.	0–13		213–230		255–265		25–35		42–61		173–205		137–148		148–151		Edmonson point		Baker rocks	
n	Mean 20	STD	Mean 13	STD	Mean 28	STD	Mean 26	STD	Mean 15	STD	Mean 10	STD	Mean 24	STD	Mean 18	STD	Mean 12	STD	Mean 15	STD
SiO_2	60.86	0.58	62.16	1.47	60.33	0.58	46.31	0.49	61.10	0.46	61.49	1.01	60.77	0.90	60.87	0.79	65.37	0.61	65.65	0.60
TiO_2	0.36	0.09	0.46	0.42	0.38	0.11	3.46	0.30	0.33	0.07	0.51	0.05	0.47	0.16	0.38	0.10	0.27	0.04	0.27	0.05
Al_2O_3	15.01	0.44	16.61	0.47	16.00	0.29	15.84	0.42	14.66	0.53	15.88	1.17	16.39	0.28	16.54	0.32	15.16	0.29	15.20	0.24
FeO	6.60	0.45	4.23	0.94	6.15	0.20	11.06	0.25	6.88	0.51	5.44	0.58	5.68	0.25	5.67	0.34	4.80	0.21	4.79	0.18
MgO	0.08	0.03	0.35	0.32	0.11	0.07	4.38	0.30	0.07	0.05	0.18	0.11	0.22	0.12	0.14	0.06	0.15	0.04	0.15	0.06
MnO	0.24	0.06	0.15	0.08	0.26	0.05	0.19	0.04	0.26	0.07	0.21	0.09	0.21	0.05	0.21	0.07	0.01	0.02	0.01	0.03
CaO	0.92	0.17	1.35	0.54	1.15	0.15	8.28	0.37	0.84	0.06	1.20	0.26	1.17	0.29	1.03	0.17	1.16	0.04	1.15	0.06
Na_2O	8.12	0.51	6.13	0.94	7.73	0.43	5.07	0.19	7.69	0.28	6.63	0.34	8.02	0.77	8.23	0.69	5.61	0.95	5.56	0.62
K_2O	4.84	0.20	5.26	0.21	5.03	0.15	2.43	0.26	4.86	0.22	5.10	0.26	5.08	0.21	5.06	0.16	4.84	0.26	4.90	0.13
P_2O_5	0.04	0.03	0.13	0.12	0.06	0.04	1.18	0.10	0.04	0.02	0.06	0.06	0.09	0.05	0.05	0.04	0.05	0.05	0.03	0.07
Total	97.10	0.66	96.85	0.68	97.24	0.77	98.24	0.69	96.77	0.39	96.73	0.57	98.13	0.71	98.22	0.09	97.47	1.75	97.76	0.97

n number of analyses, *std*: standard deviation, *cm b.s.f.* cm below sea floor

constant in the ^{40}Ar-^{39}Ar method makes the age of an unknown sample nearly insensitive to the value adopted but strongly dependent on the value used for the age of the fluence monitor. Adopting an age of 28.62 Ma for the TCs standard, as proposed by Renne et al. (2010), increases ages by only ~1 %, falling within errors in all cases. Data corrected for post-irradiation decay, mass discrimination effects, isotopes derived from interference reactions and blanks are listed in Table 3, and Online Resource 2. Errors are given as 2σ.

Data

Tephra characterization

Most of the studied samples (56 out of 64) represent volcanogenic sedimentary deposits (terminology after McPhie et al. 1993) resulting from post-eruptive, long transport and reworking of volcanic particles (pumice to scoria and lava fragments) including significant mixing with variable amounts of non-volcanic detrital grains (metamorphic and intrusive rocks, loose crystals of various mineral phases and bioclasts) and modification of primary clast shapes (e.g. clast rounding). These deposits were not considered suitable for correlation and dating purposes due to their high degree of reworking.

Eight samples from four of the nine studied cores (Fig. 2) show sedimentological features of primary pyroclastic falls to resedimented volcaniclastic deposits (terminology after McPhie et al. 1993). Deposits range in thickness from a few cm up to ~30 cm and are massive to faintly normal graded. Beds have non-erosive, sharp, sometimes irregular basal contacts and gradational to diffuse tops often affected by bioturbation (typical of submarine tephra layers; Fisher and Schmincke 1984), resulting in sand-silt lenses engulfed in a muddy matrix. Deposits are mainly composed of ash- to lapilli-sized pyroclastic fragments consisting of frothy to tubular pumice, minor blocky and dense glass shards, dark vesicular scoria, loose magmatic crystals and variable amounts of lithic particles (Fig. 3). The pyroclastic particles in each sample display a strong geochemical homogeneity (see below) and most of loose, magmatic crystals are euhedral and often preserve a coating of highly vesicular glass (with the same composition of the glass within pyroclastic fragments) adhering to crystal surfaces. These features suggest the absence of significant mixing of pyroclastic material with grains from other sources and indicate that pyroclastic particles were not affected by significant abrasion during the transport (Carey and Sigurdsson 1978). Nevertheless, minor enrichment in non-juvenile material and incipient juvenile clasts (pumice) rounding occurs in some of the deposits and indicates that original pyroclastic fall deposits may have been transported and resedimented only a limited distance, e.g. by

Table 3 Summary of ^{40}Ar-^{39}Ar results

Sample	Total crystal yield mg	Total number of analyses	Minimum age from single grains ka	±2σ[a]	Minimum error-weighted mean ka	±2σ[a]	MSWD[b]	Number of analyses	Age of deposition ka	±2σ
NW2-3.5-4.5	15	3	22.6	6.0	23.7	5.3	0.49	2	24.7	5.3
NW2-225-226	>100	11	64.7	8.0	72.0	2.8	0.89	11	72.0	2.8
NW2-256-257	94	11	74.1	4.1	74.6	2.1	0.65	8	74.6	2.1
NW31-51-52	24	6	16	15	21.2	6.4	0.24	4	≤27.6	–
NW31-69-70	22	4	18	19	–	–	–	–	≤37	–
NW3-197-199	56	11	138.7	4.0	137.1	3.4	1.09	6	137.1	3.4
AV43-138-139	<10	3	–	–	–	–	–	–	<750	–
AV43-149-150	27	5	21	17	9.7	5.3	1.96	3	≤12	–

[a] ±2σ internal error

[b] Mean square of weighted deviations

short-lived gravity-driven sediment flows or bottom currents. Conversely, the origin of these deposits by long run-out turbidity currents (either by primary pyroclastic influx or after subaerial fluvial/glacial reworking) seems very unlikely because of the absence of traction sedimentary structures, as observed in ash turbidites (Schneider et al. 2001).

On the basis of this limited degree of reworking, we consider also resedimented volcaniclastic deposits meaningful as chronological marker and thus, we selected them for tephrostratigraphic and geochemical analysis and dating purposes.

The main sedimentological and textural features, as well as the components of the identified primary pyroclastic fall deposits, are described in the following.

Core ANTA02-NW2 [Lat. (S) 73° 5.16; Long. (E) 170° 55.07; Depth b.s.l. 588 m]

NW2-0-13 is a 13-cm-thick, poorly sorted, ungraded coarse ash ($\sigma\varphi$=2.68; Mdφ=0.97) with dispersed <1 cm pumice clasts (Fig. 3a). The basal contact with dark volcaniclastic sand is sharp to diffuse and irregular. Juvenile components include white to grey, angular to subangular pumice (77 vol.%) from frothy to tubular in shape (Figs. 3a, 4a–c, and 5a–c). Pumice occasionally contains mm-sized feldspar crystals (Fig. 5a). There are loose crystals of feldspar (<3 vol.%; Fig. 5e) and rare pyroxene (Fig. 3a) coated by pumice. Lithic fragments (20 vol.%) consist of subangular scoria (commonly showing traces of abrasion and slight surface alteration), subrounded to rounded holocrystalline rocks (granitoids), oxidized lavas and loose olivine and amphibole crystals.

NW2-213-230 is a 17-cm-thick massive bed of well-sorted medium ash ($\sigma\varphi$=1.43; Mdφ=1.44). The bed is normally graded. The basal contact with volcaniclastic sand is sharp and irregular, while the upper contact again with a volcaniclastic sand is diffuse. The juvenile component consists of microvesicular to frothy (Figs. 4d and 5d), subangular, white to grey pumice (80.5 vol.%) and abundant (~8.5 vol.%) pristine crystals of feldspar, clinopyroxene and amphibole often coated by pumice (Figs. 3b and 5e, f). The lithic component (11 vol.%) consists of scarce subangular fragments of scoria and lava, loose crystals of feldspar (subrounded and milky), pyroxene and amphibole (rounded and abraded) and fragments of holocrystalline rocks (mostly consisting of feldspar; Fig. 3b).

NW2-255-265 is a massive, up to 10-cm-thick lens within grey mud, and consists almost entirely of poorly sorted coarse ash ($\sigma\varphi$=2.27; Mdφ=0.42) with dispersed <1 cm angular pumice (Fig. 3c). The juvenile component (98 vol.%) includes highly vesicular pumice with almost spherical to tubular vesicles (Figs. 4b, c and 5b–d). Some pumice clasts bear feldspar crystals <3 mm in size and

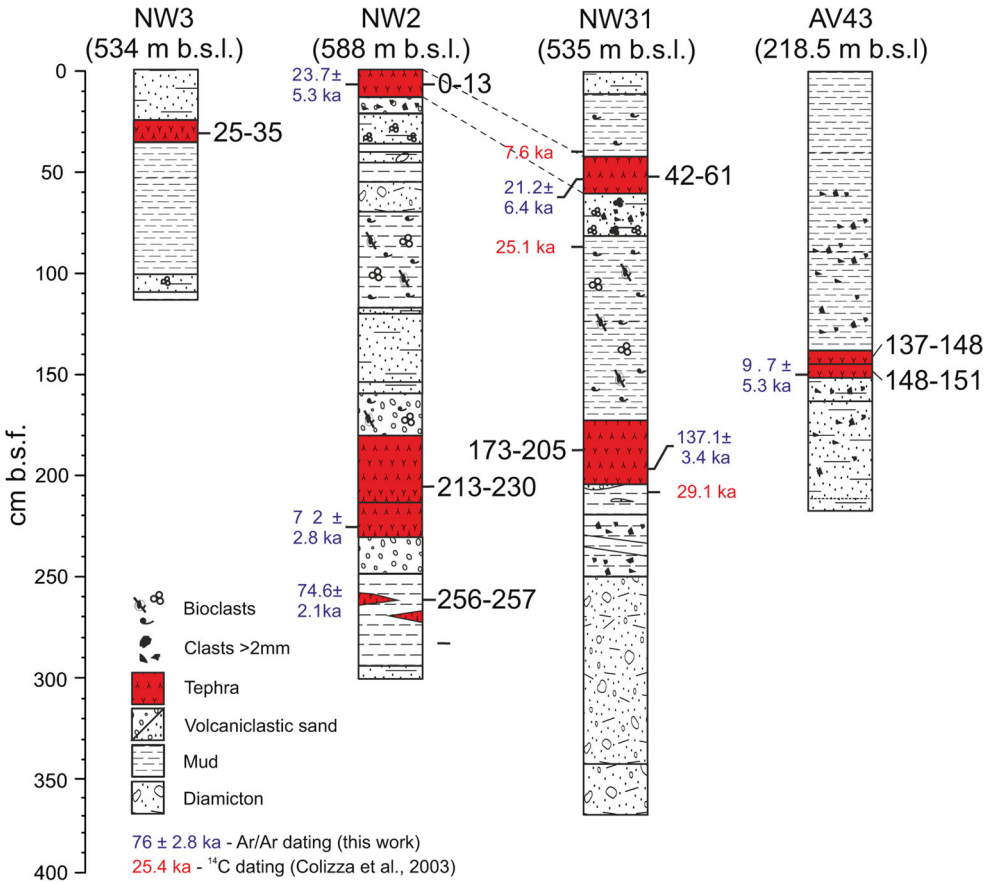

Fig. 2 Stratigraphic logs of the studied cores ^{40}Ar-^{39}Ar (this study) and ^{14}C ages (in *red*) for studied deposits from Colizza et al. (2003) are *highlighted*; b.s.l.: below sea level

tiny acicular clinopyroxene crystals. Lithic fragments are scarce (<2 vol.%) and consist of subangular scoria, holocrystalline rocks (granitoids) and subrounded crystals of milky feldspar (Fig. 3c).

Core ANTA02-NW3 [Lat. (S) 72° 58.02; Long. (E) 170° 59.34; Depth b.s.l. 534 m]

NW3-25-35 is a ~10-cm-thick bed composed of well-sorted medium ash ($\sigma\varphi$=1.64–1.70; Mdφ=1.36–1.42). The bed is normally graded with a sharp and concave basal contact against sandy mud; the top grades into stacked mm- to cm-thick layers of a well- to poorly sorted coarse to medium ash ($\sigma\varphi$=1.37–2.38; Mdφ=0.62–1.67) set in a muddy matrix and commonly containing oversized clasts up to 5 mm in diameter. The juvenile component (88 vol.%; Figs. 3d and 4e, f) consists of blocky and variably vesicular (low to moderate) glassy particles, pale yellow to dark brown in colour and equant in shape with microlites of plagioclase, olivine and oxide (Fig. 5g, h) and frothy to fluidal fragments, moderately to highly vesicular, with microphenocrysts of clinopyroxene and olivine immersed in a groundmass rich in plagioclase microlites. Scarce (<1 vol.%) loose crystals of plagioclase occur (Fig. 3d). Lithic fragments are abundant (11 vol.%; Fig. 3d) and include subangular pumices and scoria, rounded fragments of tuff and abundant holocrystalline rocks. Two main mineral assemblages were identified within the holocrystalline rock fragments; the first consists of quartz, K-feldspar, plagioclase, oxides±orthopyroxene, the second of plagioclase, clinopyroxene, oxides±nepheline. Most lithic fragments show variable degrees of alteration with the original minerals substituted by clays. Loose crystals of clinopyroxene, olivine and feldspar also occur.

Core ANTA99-NW31 [Lat. (S) 73° 13.53; Long. (E) 170° 59.28; Depth b.s.l. 535 m]

NW31-42-61 is a 19-cm-thick, normally graded bed consisting of a poorly sorted, very coarse to medium ash ($\sigma\varphi$=2.1–2.3; Mdφ=−0.6–1.0) with scattered, oversized angular to subangular pumice (up to 2 cm). The basal contact with underlying clayey sand and the top contact with silty mud are both sharp. Juvenile clasts (~91 vol.%; Fig. 3e) include greenish dense glass fragments (Figs. 4g, h and 5i) and highly vesicular, pale grey pumice with vesicles ranging in shape from elliptical to tubular (Figs. 3e and 5b, c). There are a few (<3 vol.%) crystals of feldspar and clinopyroxene wetted by pumice. The lithic component (~5 vol.%) consists of subangular fragments of lava and holocrystalline rocks (chlorite metamorphic schist) and loose crystals of feldspar and clinopyroxene (Fig. 3e).

NW31-173-205 is a 32-cm-thick bed composed of poorly sorted (σφ=2.12–2.24) very coarse to medium ash (Mdφ=−0.71–1.59) with abundant <2 cm, angular to subangular pumice especially in the lowermost part of the deposit. The basal contact with massive mud is sharp and slightly irregular, while the upper contact with mud is sharp and horizontal. The juvenile component (~72 vol.%; Fig. 3f) consists of white to pale grey pumice (almost aphyric) and scarce, dense fragments of greenish glass (Figs. 4g, h and 5i). Ash and pumice are highly vesicular with vesicles ranging in shape from microvesicular to frothy and tubular (Figs. 4a–d and 5b–d). There are a few (<4 vol.%) loose crystals of feldspar coated by pumice (Figs. 3f and 5e).

Lithic fragments are abundant (~24 vol.%) and comprise subangular scoria often altered to zeolite, holocrystalline rocks mainly consisting of plagioclase, clinopyroxene, spinel and alkali feldspar, tuff with perlitic texture, fragments of volcaniclastic siltstone and loose crystals of subrounded milky feldspar and quartz (Fig. 3f).

Core ANTA02-AV43 [Lat. (S) 74° 8.45; Long. (E) 166° 4.97; Depth b.s.l. 218.5 m]

AV43-137-148 is an 11-cm-thick, well to poorly

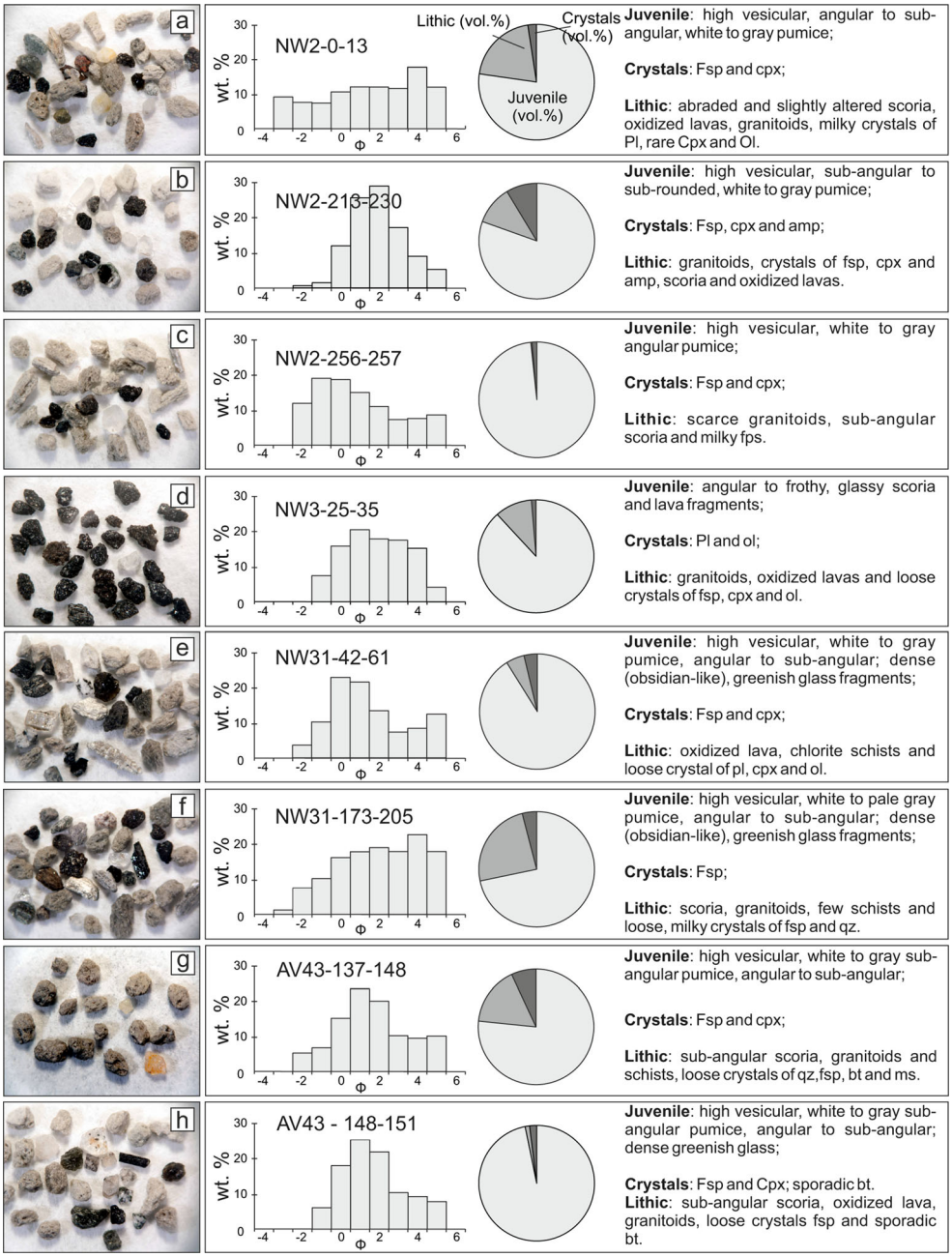

Fig. 3 Images of grains from tephra layers with grain size distribution, main component abundances (vol. %) and description. Illustrated clasts are of grain size class phi-1. 'Crystals' coated by glass with the same composition of the glass within pumice are of inferred primary origin. *Fps* feldspar, *Cpx* clinopyroxene, *Pl* plagioclase, *Ol* olivine, *Amp* amphibole, *Qz* quartz, *Bt* biotite, *Ms* muscovite

sorted (σφ=1.57–2.02), medium to fine ash (Mdφ= 1.21–2.4). The bed is normally graded. The basal contact with primary pyroclastic fall (AV43-148-151) is sharp, and the upper contact with massive mud is sharp and horizontal. The juvenile component includes white to pale grey subangular pumice (77 vol.%; Fig. 3g) and abundant (~7 vol.%) feldspar crystals (Figs. 3g). Pumice are highly vesicular and microvesicular to tubular (Figs. 4b–d and 5b–d). The abundant lithic fragments (16.5 vol.%) include subangular fragments of highly crystallized lava and two different types of holocrystalline rocks; the first type consists of plagioclase, biotite, apatite and quartz, the second of K-feldspar, plagioclase, biotite and loose crystals of quartz, as well as subrounded, milky feldspar and loose muscovite and biotite laminae (Fig. 3g).

AV43-148-151 is a 3-cm-thick, well-sorted (σφ= 1.74) medium ash (Mdφ=1.23). The bed consists almost entirely of juvenile clasts (96.5 vol.%) comprising angular to subangular, white to pale grey pumice and scarce greenish vesicle-free glass (Figs. 3h and 5i). The basal contact with sand and the upper contact with AV43-137-148 tephra is very sharp and almost flat. Pumice is highly vesicular and microvesicular to tubular (Fig. 4b–d). There are a few (~2 vol.%) crystals of feldspar and clinopyroxene, along with sporadic biotite-rich laminae (Fig. 3h). Lithics are very scarce (~1 vol.%) and include subangular scoria fragments, holocrystalline rocks

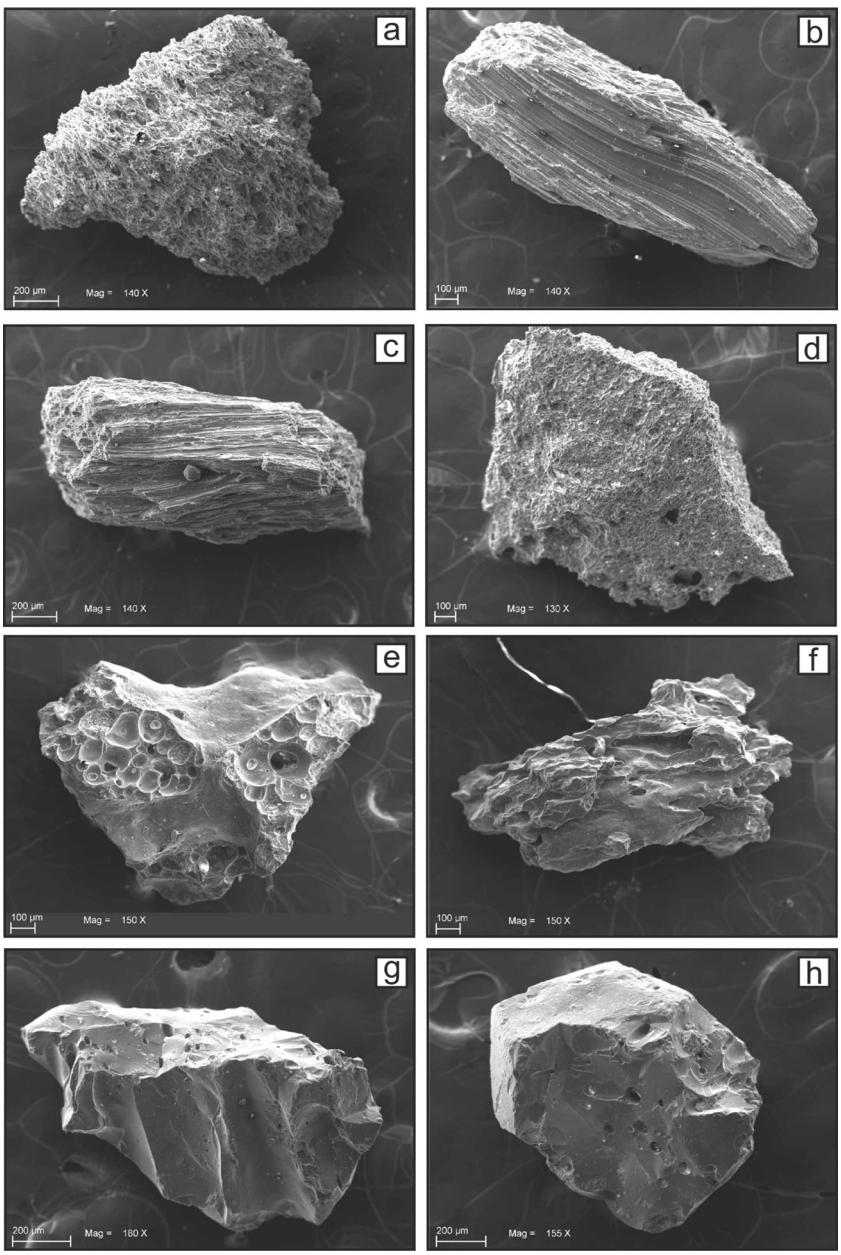

Fig. 4 Scanning electron microscope secondary electron (SEM-SE) images representative of textures identified in studied primary pyroclastic and resedimented volcanic deposits. **a** Highly vesicular, frothy pumice fragments (NW02-0-13); **b**, **c** highly vesicular, blocky pumice with tubular vesicles (NW2-255-256); **d** highly vesicular (microvesicular), blocky pumice (NW2-213-230); **e**, **f** moderately vesicular, glassy scoria with **f** fluidal texture (NW3-25-35); **g**, **h** almost vesicle-free glass fragment (AV43-148-151)

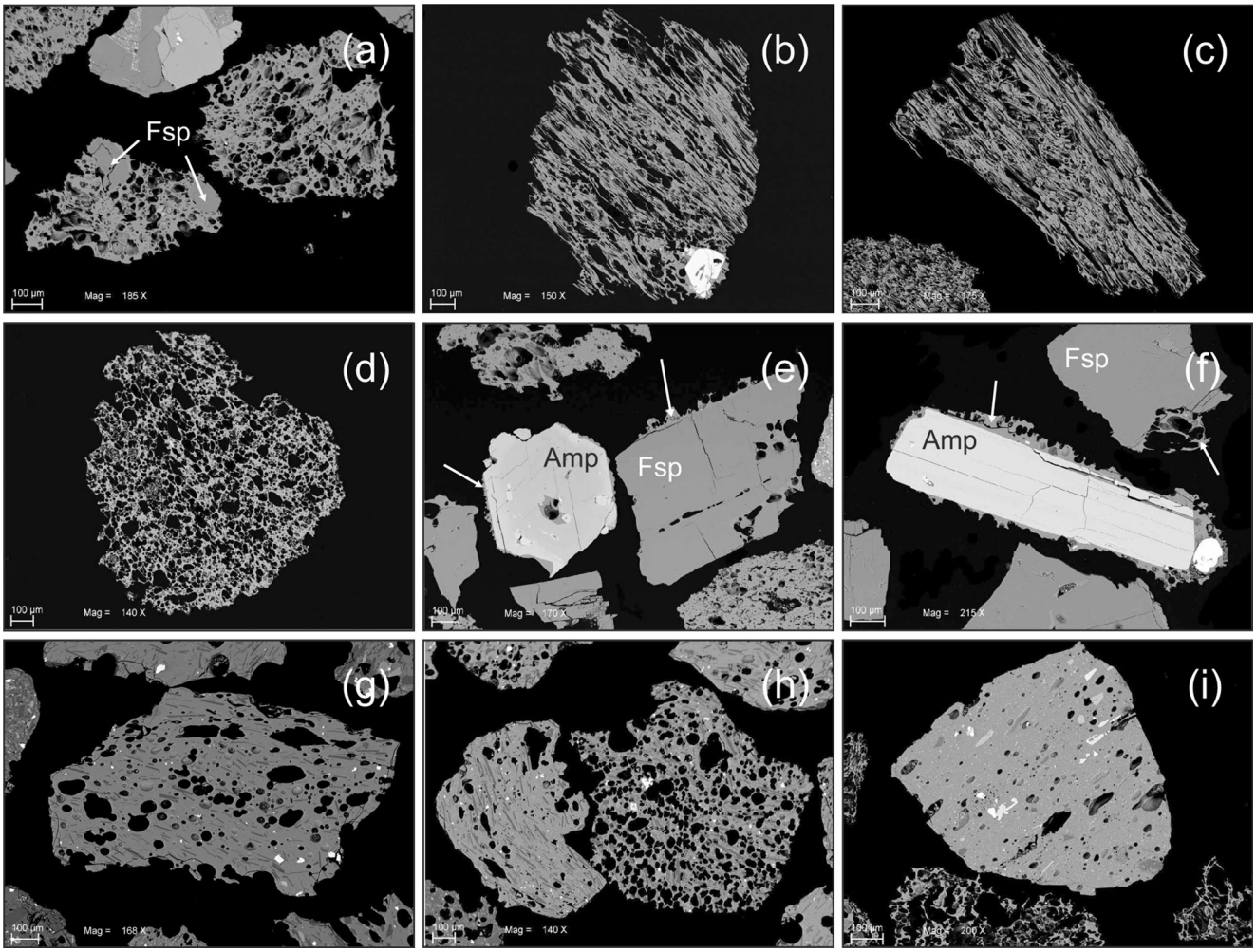

Fig. 5 Scanning electron microscope secondary electron (SEM-BSD) images representative of textures identified in studied primary pyroclastic and resedimented volcanic deposits. **a** Frothy pumice with feldspar microphenocrysts (NW2-213-230); **b**, **c** tubular pumice (AV43-148-151 and NW31-42-61); **d** highly, microvesicular pumice (NW31-173-205); **e**, **f** loose magmatic crystals of amphibole and feldspar coated by vesicular glass (NW2-255-256); **g**, **h** blocky, low-vesicular, basaltic fragment with glassy groundmass containing microlites of plagioclase, olivine and oxide (NW2-25-35); **h** moderately vesicular, basaltic fragments with plagioclase microlite-rich groundmass (NW2-25-35); **i** low-vesicular, blocky glass fragment (NW31-42-61)

fragments (granitoids) and loose crystals of feldspar and sporadic biotite (Fig. 3h).

Glass and mineral composition

The major element composition of analysed glass and minerals are shown in Fig. 6 and Table 2 and in Fig. 7, respectively. Only clear and euhedral to subhedral crystals were selected for analyses in order to avoid non-juvenile minerals when possible selecting those coated by volcanic glass. Crystals in Fig. 3 are those coated by glass with the same composition of the glass within pumice and were considered representative of pumice mineral assemblage. Three of the samples from Mount Melbourne volcano were holocrystalline and not suitable for glass groundmass microprobe analysis. Only two of the five samples from Mount Melbourne volcano, G03 and G62, have glassy groundmass suitable for microprobe analyses, although with a significant amount of microlites of alkali feldspar.

Most tephra beds consist of a single, homogeneous glass population (Table 2 and Fig. 6). The majority of samples are evolved rocks plotting in the trachyte field of the TAS diagram (SiO_2=60.8–66.6 wt.%; Na_2O+K_2O=11.2–13.8 wt.%). The major element compositions of glass in the studied samples from sediment cores form at least four compositional groups within the Harker and K_2O vs. Na_2O wt.% classification diagrams (Fig. 6).

Samples NW2-0-13 and NW31-42-61 are chemically indistinguishable from one another and can be discriminated from the other samples by their low Al_2O_3 content and slightly high FeO_{tot} content, as indicated in Fig. 6c. Loose crystals in equilibrium with these glasses are anorthoclase $Ab_{58–65}$, $Or_{40–32}$, $An_{2–4}$ and

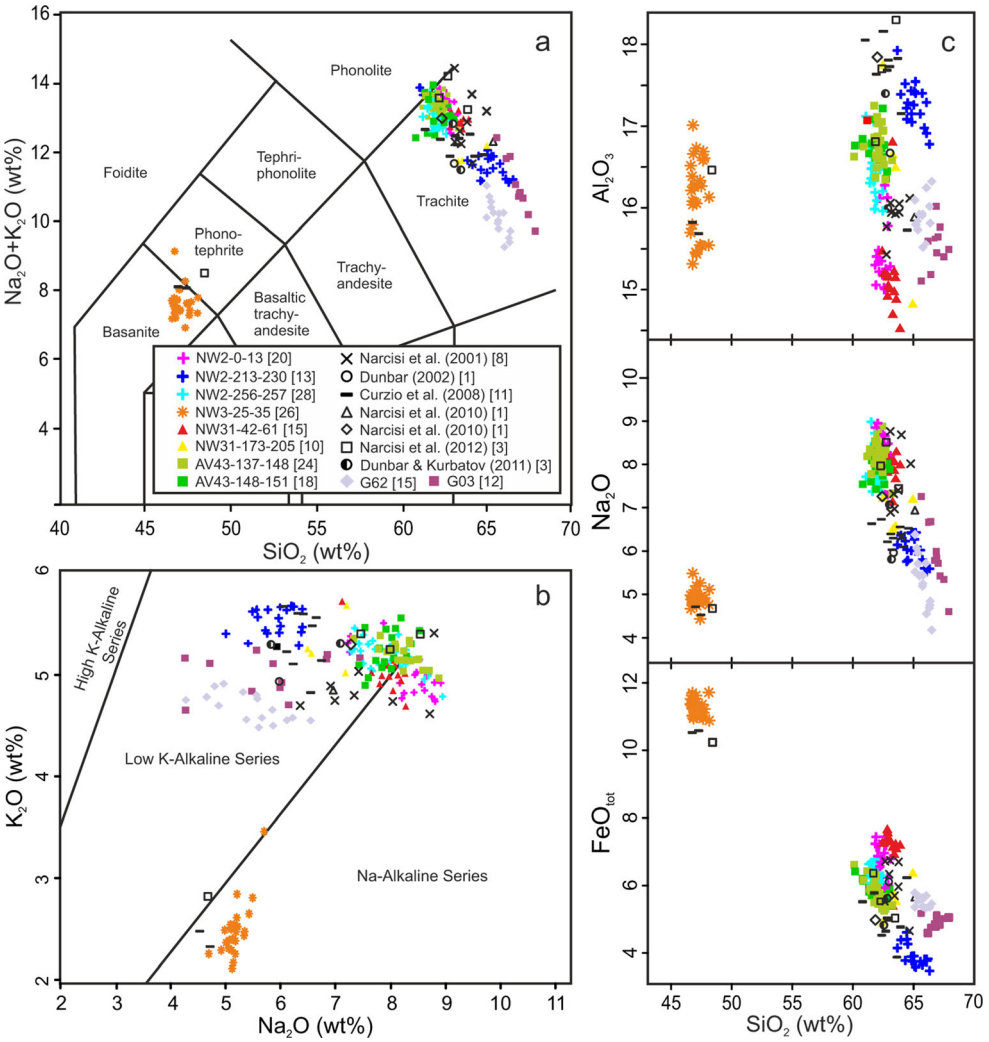

Fig. 6 Glass compositions of the primary pyroclastic fall, resedimented volcaniclastic deposits identified in the studied cores and samples G03 and G62 (coloured full symbols) from Edmonson Point and Baker Rocks, respectively (Giordano et al. 2012). These are plotted against comparable glass compositions available in literature for crypto- and micro-tephra recovered in ice cores and for ash layers in blue ice from the Frontier Mountain. The number of analyses plotted for studied and reference samples are reported in *square brackets*. Analyses were normalized to 100 % on a volatile-free basis. **a** Total alkali-silica diagram of Le Bas et al. (1986); **b** classification of the glass composition in a K_2O vs. Na_2O wt.% diagram; **c** Harker diagrams

clinopyroxene $Fs_{20–30}$ (Fig. 7). Other loose crystals of differing compositions, more abundant in NW2-0-13, are apparently reworked (slightly abraded and opaque) plagioclase (An_{25-90}), clinopyroxene (Fs_{11-16}; Fig. 7) and olivine ($Fo_{70–86}$) coated by less evolved glass, and rare kaersutitic amphibole.

Sample NW2-213-230 stands out for a high silica content and an overall low alkali content, Na_2O especially (Fig. 6b). Minerals in equilibrium with glass are anorthoclase ($Ab_{60–65}$, $Or_{28–36}$, $An_{4–7}$), clinopyroxene ($Fs_{28–41}$, $Wo_{41–45}$; Fig. 7) and ferropargasitic amphibole (Mg# 0.28–0.44, Si in formula 6.1–6.4). Less calcic anorthoclase crystals ($Ab_{67–71}$, $Or_{28–32}$, $An_{<1}$) are interpreted as lithic clasts.

AV43-137-148 and 148–151 and NW2-255-265 show virtually the same glass composition and mineral chemistry (Fig. 6a–c). Loose crystals in equilibrium with the glass are mainly anorthoclase $Ab_{59–68}$, $Or_{30–40}$ and An<4 associated with minor Fe-rich clinopyroxene ($Fs_{40–50}$, Fig. 7). AV43-148-151 also contains local biotite crystals.

The composition of layer NW31-173-205 is intermediate to that of NW2-213-230 and other trachytic samples (Fig. 6a–c) and shows a wide range of Al_2O_3 contents. Pumice bears anorthoclase crystals that are slightly less potassic than in NW2-213-230 ($Ab_{55–58}$, $Or_{43–36}$) but have similar calcium contents ($An_{2–6}$, Fig. 7).

The composition of glass in sample NW3-25-35 plots in the basanite field (CIPW normative olivine=11.86 %; SiO_2=46.6–48.1 wt.%; Na_2O+K_2O=7.1–8.2 wt.%; Fig. 6a) and shows a sodic affinity (Fig. 6b). Glass fragments contain <1 mm crystals of $Fo_{80–84}$ olivine with tiny (<10 μm)~Fo_{76} rims, $Fs_{11–17}$ clinopyroxene <0.5 mm in diameter and rare microphenocrysts of andesinic plagioclase (Fig. 7). Loose large Na-rich plagioclase and alkali feldspar are lithic clasts.

The composition of glass in samples G03 and G62 from Edmonson Point and Baker Rocks (Mount Melbourne) are low K-alkaline trachytes similar to those of NW02-213-230 and NW31-173-205 but with slightly differing Al contents.

Both samples show short compositional trends that are consistent with the glass groundmass being residual (mainly depleted in alkali content) after a variable crystallization of alkali feldspar microlites.

^{40}Ar-^{39}Ar data

Alkali feldspars suitable for ^{40}Ar-^{39}Ar dating were selected under a binocular microscope on the basis of their petrologic characteristics, e.g. clear appearance, low degree of abrasion and presence of fresh glass coating the crystals.

Grains of alkali feldspar were recovered from sample NW2-0-13 (sampled at 3.5–4.5 cm depth) for a total weight of ~15 mg. Grains were split into three aliquots, one of which consisted of a single large grain yielding ages ranging nominally from ~23 to ~125 ka. Two of the three ages overlap within error, yielding an error-weighted mean age of 23.7± 5.3 ka. The youngest nominal value was obtained on the single grain (22.6±6.0 Ma, ±2σ analytical error; Online Resource 2). Mineral separates from layer NW2-213-230 (sampled at 225–226 cm depth) contained several euhedral to subhedral alkali feldspar grains that were generally too small for single-grain analysis. Total fusion experiments were mainly performed on splits consisting of a few (2 to 4) crystals; in a cumulative probability distribution plot (Fig. 8), data show a single-mode distribution and yield an error-weighted mean age of 72.0±2.8 ka (±2σ internal error, MSWD=0.89; Online Resource 2). The slightly deeper layer from the same core, NW2-255-265 (sampled at 256–257 cm depth), similarly to layer NW2-213-230, yielded several alkali feldspar crystals that were large enough for single-grain analysis (Online Resource 2). Eight of the eleven analyses define a narrow range of ages, yielding a statistically acceptable error-weighted mean age of 74.6±2.1 ka (±2σ internal error, MSWD=0.65) that is indistinguishable at the 2σ level from the age of the upper layer. Two further analyses gave ages overlapping at ~110 ka, whereas a third performed on a single grain yielded an age of 80.7±4.3 ka (±2σ analytical error).

Sample NW31-42-61 (sampled at 51–52 cm depth) yielded an alkali feldspar concentrate of ~24 mg that was split into six aliquots. One run attempted on a single grain yielded a poorly defined age of 16±15 ka. The analysis of thirteen whitish grains yielded an age of ~280 Ma and a low K/Ca ratio (Online Resource 2), indicating that the split included plagioclase grains. The remaining splits yielded ages ranging nominally from 19 to 52 ka that are affected by large analytical uncertainties due to the low gas yield. In a cumulative probability plot (Fig. 8), four data points define a main peak yielding an error-weighted mean age of 21.2±6.4 ka (MSWD= 0.24) that is statistically indistinguishable from the ~24 ka-age of layer NW2-0-13, whereas a single analysis defines a small peak at ~50 ka. A good feldspar concentrate was obtained from sample NW31-173-205 (sampled at 197–198 cm depth, with a total weight of 56 mg). Crystals were split into eleven aliquots, two consisting of single grains (Table 2, Online Resource 2). Data yield ages ranging nominally

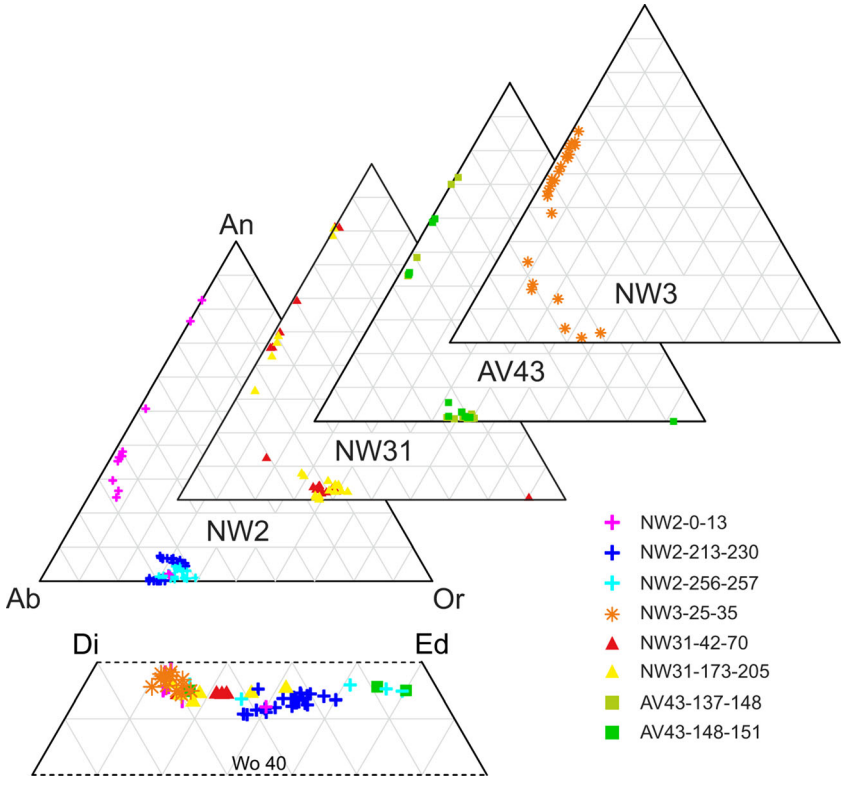

Fig. 7 Composition of feldspars and clinopyroxenes from the analysed tephra layers

from ~130 to 215 ka and defines three peaks in a cumulative probability plot (Fig. 8): the youngest with an error-weighted mean of 137.1±3.4 ka (n=6, MSWD=1.1; Online Resource 2), an intermediate one at ~155 ka and the oldest at ~215 ka.

Layers from core AV43 yielded few crystals: less than 10 mg from sample AV43-137-148 (sampled at 138–139 cm depth) and ~25 mg from sample AV43-148-151 (sampled at 149–150 cm depth). Analyses were performed in three runs (Online Resource 2). One was performed on turbid whitish grains and gave a Paleozoic age with a low K/Ca ratio. Two other analyses yielded ages of 0.73±0.3 Ma and 1.2±0.2 Ma. The feldspar separate of sample AV43-148-151 was split into five aliquots. In a cumulative probability plot, age data define a distinct peak (n=3, Fig. 8) yielding an error-weighted mean of 9.7±5.3 ka, and single data points define small peaks at ~170 and 280 ka. One analysis performed on a single grain gave a poorly defined age of 21±17 ka.

Table 3 summarizes the ^{40}Ar-^{39}Ar data presented above and for each sample lists the age of deposition for each layer. For samples characterized by a low crystal content (namely NW31-51-52, AV43-138-139 and AV43-148-151) and consequently by age data affected by large uncertainties, we conservatively indicate a maximum age based on the youngest error-weighted mean ages and the relative 2σ internal error (Table 3).

Discussion

On the basis of sedimentological characteristics, the high abundance of volcanic particles and small quantity of non-volcanic detritus, as well as the homogeneous chemical composition of glass, eight primary pyroclastic falls to slightly resedimented volcaniclastic deposits were identified in four of the nine studied cores (NW31 and NW2, NW3 and AV43). These deposits mostly consist of pumiceous lapilli and ash, with minor amounts of loose magmatic crystals and lithic fragments. The majority of the studied deposits have trachytic compositions, with only the NW3 tephra consisting of scoriaceous lapilli and ash of basanitic composition.

Implications for eruptive style

Tephra thickness and granulometry, including the maximum size of lithic and juvenile clasts, systematically measured in a

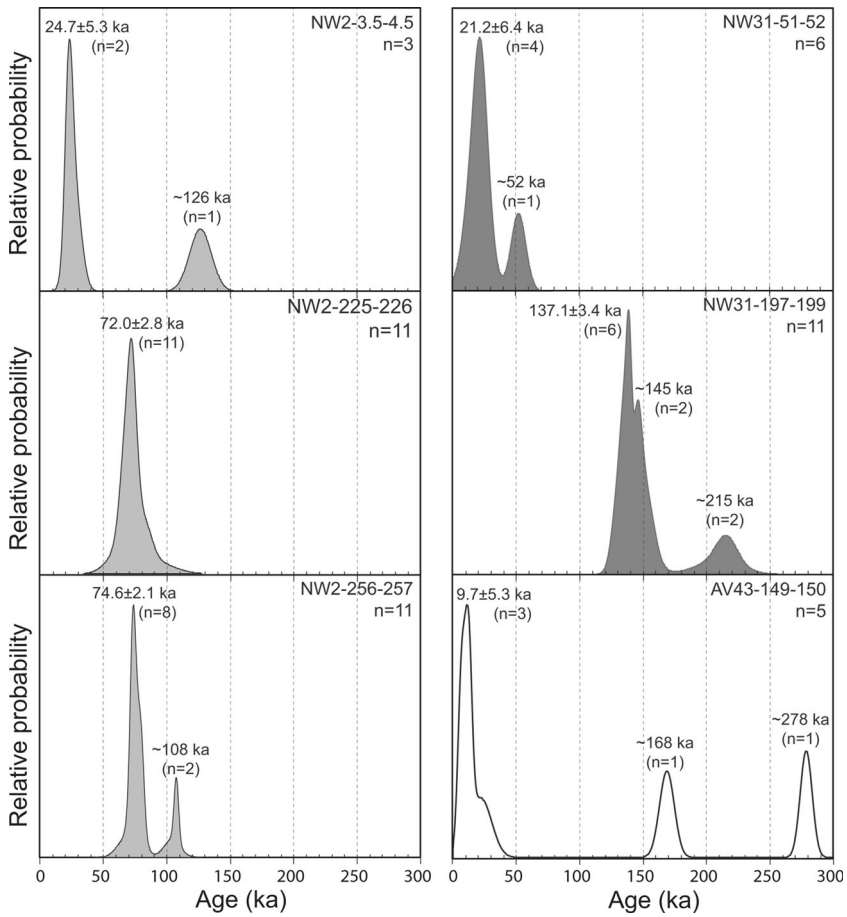

Fig. 8 Cumulative probability distribution of ages from total fusion experiments on alkali feldspar separates. Uncertainties on the error-weighted mean ages also include the error in the J values. (n) refers to the number of runs

number of exposures are normally used to infer eruption source parameters such as eruptive column height, total mass ejected, mass discharge rate, etc. The morphology of volcanic particles can provide clues on how the particles formed (i.e. fragmentation mechanism and eruption dynamics), on parameters such as magma viscosity and volatile content, on interaction with external water (sea, freshwater or ice) and on the post-fragmentation history of juvenile fragments (e.g. abrasion for long distance reworking/transport).

In the case of the studied deposits, it was impossible to obtain a rigorous estimate of eruption parameters without knowing how the physical characteristics of the deposits varied with distance from the eruptive centre. Our results may nonetheless help to qualitatively assess the eruptive style and intensity of the volcanic eruptions that produced these pyroclastic fallout deposits.

Considering that layers are tens of centimetres-thick, that some of the tephra contain medium-sized lapilli and that sampling sites are at least 50 km (up to >200 km) from any known (subaerial) volcanic centre, we infer that they were deposited during high-energy subplinian to plinian eruptions able to produce an eruptive column of several km and to disperse lapilli and ash over large distances (Carey and Bursik 2000). This also taking into account that the dispersion of pyroclastic fall products might have been influenced by the westerly prevailing winds (Fig. 1; Connolley and King 1993) and thus that the studied deposits might represent the thickest deposits in proximity to maximum dispersal axis.

As mentioned above, volcanic particles identified in the studied tephra show a variety of morphologies: they are mostly highly vesicular pumice with only minor amounts of poorly vesicular to vesicle-free particles. Loose magmatic crystals are also abundant. Pumice range in shape from frothy to elongated and have spherical, elongated to tubular vesicles whereas poorly vesicular to dense vitric particle are mostly blocky. Loose magmatic crystals are coated by highly vesicular glass with the texture and same geochemical composition of the pumices. Particles morphology and texture, including those of magmatic crystals, likely suggest that the studied deposits originated mostly by magmatic fragmentation (exsolution of dissolved volatiles) during explosive eruption, and that there are few hydroclastically fragmented pyroclasts for the interaction of magma with ground water or ice (Heiken and Wholetz 1985; Buettner et al. 1999).

The morphology and texture observed in the scoria lapilli and ash from the ANTA02-NW3 core are vice versa typically generated by weakly to mildly explosive basaltic eruptions (Cashman et al. 2000). The contemporary occurrence of vesicular, frothy to fluidal and blocky particles may suggest that a combination of magmatic and hydromagmatic fragmentation cannot be ruled out. The dispersal of fallout from this kind of eruption is usually more limited with respect to plinian and subplinian eruptions, implying a more local unknown volcanic source.

Possible volcanic sources for Ross Sea tephra

^{40}Ar-^{39}Ar results constrain the possible volcanic sources to those active between ca. 137 and 12 ka (Table 3). Since all the studied beds are well-preserved pyroclastic fall deposits with thicknesses of the order of several to tens of centimetres and relatively coarse grain size, we considered the northern Victoria Land volcanoes as probable sources because they are the closest volcanic edifices to the coring sites. The potential sources must have yielded products in this time frame with eruptive style and geochemical composition similar to those of the tephra. Volcanoes that fulfil these conditions are Mount Melbourne, Mount Rittmann, The Pleiades volcanic complexes and more to the south, Erebus volcano. Mount Melbourne volcano has been very active since 150 ka (Giordano et al. 2012). Late Pleistocene to Holocene deposits crop out in different portions of the edifice and consist of trachytic ignimbrites (123.6±6.0 ka; Giordano et al. 2012), alkali basaltic, hawaiitic and subordinate benmoreitic lavas and scoria cones (90.7±19.0 ka; Giordano et al. 2012). The most recent products of Mount Melbourne are exposed widely on the edifice and consist of trachytic to rhyolitic pumice fall deposits likely originated from plinian-scale eruptions (Giordano et al. 2012). Mount Rittmann volcanic activity dates between 3.97 and 0.07 Ma (Armienti and Tripodo 1991; Perchiazzi et al. 1999). Recent activity is still poorly known due to the scarcity of outcrops. It is unknown if the volcano has been active in the recent past. K-Ar ages for Mount Rittmann effusive products of phonolitic or trachytic composition yield ages of 240±200, 170±20 and 70±20 ka (Perchiazzi et al. 1999). The fumaroles and geothermal activity discovered on the summit part of the volcano (Bonaccorso et al. 1991) suggest that the volcano is dormant but not extinct. The Pleiades volcanoes have been very active over the last 100 ka. (Esser and Kyle 2002). ^{40}Ar-^{39}Ar ages indicate that the most recent volcanic activity occurred at 6±6 ka (Esser and Kyle 2002) and that volcanism in this area is as old as 847 ka. K-Ar data gives even more recent ages of around 3 ka (Armstrong 1978). The occurrence of hydrothermal activity (Esser and Kyle 2002; Fraser et al. 2014) and the widespread pumice lapilli fallout deposits on the surface of The Pleiades provide evidence for Holocene volcanic activity. Deposits from The Pleiades consist of rocks belonging to the alkali-rich basanite-tephrite-phonotephrite-phonolite suite (Kyle 1990) and to an alkali-poorer suite of hawaiites, mugearites, benmoreites and trachytes (1990).

Erebus volcano has been active since at least 1.3 Ma and has erupted lava varying from basanite to phonolite in composition (Kyle et al. 1992; Esser et al. 2004). The relative recent explosive activity of Erebus volcano is testified to by several tens of tephra beds embedded in ice on the flanks of the volcano or cropping out at several localities close to the volcano including at least two large eruptions that deposited

tephra ~200 km from source (Harpel et al. 2008). Late Pleistocene and Holocene activity has included anorthoclase-phyric phonolitic lava flows, caldera formation, and explosive activity including a plinian eruption forming the tephra preserved at Mount DeWitt (Harpel et al. 2004).

To identify the possible provenance of the studied tephra, we compared the composition of glass and minerals with data from the literature on the pyroclastic products of known eruptions of the above-mentioned volcanoes.

Tephra correlation has been determined on the basis of the similarity coefficient (SC) of Sarna-Wojcicki et al. (1984). The SC was calculated comparing the average major element composition (calculated on normalized concentrations) of glass in the studied tephra and those from the literature. Similarity, coefficients were calculated excluding elements with concentrations close to detection limits (Sarna-Wojcicki et al. 1984) by using this formula:

$$SC = \frac{1}{n}\sum \frac{XiA}{XiB}$$

Where: i=element number, n=number of elements, XiA=concentration of element i in sample A, and XiB=concentration of element i in sample B with XiA is the minimum of the pair XiA, XiB. SC of 0.92 is typically considered as the lowest acceptable value for tephra correlation (Froggatt 1992). SC>0.95 indicates a good correlation between a sample pair, and SC>0.97 is considered a very good correlation.

Unfortunately, there are limitations that reflect limited knowledge of the volcanology, chronostratigraphy and rock geochemistry of most Antarctic volcanoes, especially those in northern Victoria Land. Furthermore, most of the published geochemical data on known and dated eruptions of Mount Melbourne, Mount Rittmann, The Pleiades and Erebus are for bulk rock compositions, with an almost complete absence of published glass geochemistry. This makes comparison with microprobe compositions of glass difficult. It is well known that the major element composition of volcanic glass in pyroclastic products may strongly differ from the bulk rock compositions of the same volcanic products (e.g. lavas, dikes, bombs, blocks, etc.) even if taken from the same rock (Stern 1990, 2008; Kraus et al. 2013). This is because bulk rock analyses include phenocrysts with compositions different from that of the glass, which represents melt that is usually enriched in some chemical elements relative to that of the bulk rock.

Nonetheless, our analyses of pyroclastic products from Mount Melbourne highlight that at least two of the studied marine tephra layers, NW31-173-205 and NW2-213-230, are compositionally compatible with, respectively, the Edmonson Point trachytic ignimbrite (sample G03 of Giordano et al. 2012; SC=0.89) and the products of the last Mount Melbourne eruption, a plinian pumice fallout deposit of probable Holocene age (G62 of Giordano et al. 2012; SC=0.86). Although the SC value is slightly below the lowest value acceptable for tephra correlation (0.92; Froggatt 1992), we suggest that NW31-173-205 and NW2-213-230 have a compositional affinity with products of Mount Melbourne. In addition, the ^{40}Ar-^{39}Ar age of 137.1±3.4 ka for NW31-173-205 is comparable, though not overlapping within error, with that of 124.3±6.4 ka for the Edmonson Point trachytic ignimbrite (Giordano et al. 2012), and strengthen inference of a source in the Mount Melbourne volcanic complex.

We also compared the glass composition of tephra identified in the studied cores with those of englacial tephra from the study area and of micro- and crypto-tephra recovered in Antarctica during deep ice core drilling at Dome Fuji (Fujii et al. 1999; Kohno et al. 2004; Narcisi et al. 2006), Vostok Dome (Basile et al. 2001; Delmonte et al. 2004; Narcisi et al. 2010a), Siple and Taylor Domes (Dunbar et al. 2003; Dunbar and Kurbatov 2011 and references therein), EPICA Dome-C (Delmonte et al. 2004 and 2008; Narcisi et al. 2005; Narcisi et al. 2010a) and Talos Dome (Narcisi et al. 2010b and references therein).

Samples AV43-137-148 and -148-151, with an ^{40}Ar-^{39}Ar age of 9.7±5.3 ka, are contiguous in the core and chemically indistinguishable, yielding a SC value of 0.95. These probably represent deposits of two different phases of the same eruption or deposits produced by two eruptions from the same volcanic complex that occurred over a short period of time and were fed by the same magma source. These layers have a good correlation in age and composition to the TD741 (SC=0.92–0.96) and TD779 (SC=0.90–0.94) ash layers identified in the Talos Dome ice core (Narcisi et al. 2012) with inferred ages of 13.77 ±0.13 ka and 15.9±0.14 ka, respectively (Table 3). For TD741, no source has yet been suggested, whereas for TD779, derivation from Mount Melbourne has been indicated by Narcisi et al. (2012).

As mentioned above, samples NW2-0-13 and NW31-42-61 are almost chemically indistinguishable (SC=0.96) and correlate with the NW2 and NW31 cores. Unfortunately, because of the paucity of data on the composition of the volcanic glass in the northern Victoria Land, it was not possible to either correlate these deposits with their onland vent(s) or to infer the area of origin. Similarly, the remaining glass samples NW2-255-265 (trachyte) and NW3-25-35 (basanite) have only a partial geochemical affinity with the glass in some volcanic ash and tephra layers identified in Antarctic ice cores (e.g. Talos Dome, Taylor and Siple domes, Vostok Dome and Epica Dome-C) and in the blue ice of Frontier Mountain (Curzio et al. 2008) and Brimstone Peak (Dunbar 2003). Although most of these tephra have compositional affinities with the products of explosive activity at Mount Melbourne, Mount Rittmann and The Pleiades volcanic complexes (Narcisi et al. 2001; Dunbar 2002; Narcisi et al. 2006; Curzio et al. 2008; Narcisi et al. 2010a, b; Narcisi et al. 2012; Dunbar and Kurbatov 2011),

they cannot be ascribed to any one volcano or to a specific eruptions.

Conclusions

For the first time in this area, we have attempted a correlation between marine and terrestrial archives by comparing pyroclastic fall and slightly resedimented volcanic deposits recovered in cores with subaerial tephra sampled on Mount Melbourne volcano. In addition, we compared the studied tephra with micro- and crypto-tephra recovered in deep Antarctic ice cores and with englacial tephra.

Results indicate that eruptive activity in the Melbourne Volcanic Province of northern Victoria Land was intense during the Late Pleistocene-Holocene. At least five mid to high intensity (plinian to subplinian) explosive eruptions occurred in this period.

Geochemical data and ^{40}Ar-^{39}Ar ages indicate that one of these eruptions took place from the Mount Melbourne volcanic complex at 9.7±5.3 ka and two more show a geochemical affinity with this source.

As for the remaining studied tephra, the limited knowledge of the volcanology, chronostratigraphy and glass geochemistry of most volcanic centres in the Melbourne Volcanic Province only allows the identification of a general area of provenance, precluding correlation between marine tephra layers and specific source volcanoes or eruptions.

We conclude that Antarctic tephrostratigraphic records, whether marine, terrestrial or glacial, provide only a partial picture of the eruptive history of an area and cannot be used alone for volcanological reconstructions. The majority of the eruptions identified in the studied cores, though inferred to have been of high intensity, are not recorded in ice cores drilled in Antarctica and vice versa. This is because the dispersal of pyroclastic products is strongly influenced by the direction of prevailing winds.

A major obstacle in the correlation and synchronization of different records is the lack of comparable geochemical data, e.g. the composition of glass from all possible volcanic sources. A challenge for future tephrochronology research in Antarctica will be the enrichment of available geochemical datasets (e.g. AntT Project founded by National Science Foundation; http://cci.um.maine.edu/AntT/), which must include the major and trace element composition of glass from as many volcanic sources as possible. This would allow the reliable correlation and synchronization of tephra identified in records from different environments with source areas.

Acknowledgments A. Cavallo of INGV Sezione di Roma is acknowledged for assistance in microprobe analyses. This work was funded by the Italian Programma Nazionale di Ricerche in Antartide (PNRA), PdR2010/A2.12: Glacial and interglacial transitions deduced by the multidisciplinary study of marine sediments in the Ross Sea (Antarctica). A. Di Roberto benefited from a postdoctoral grant from the above-mentioned PNRA project. J.D.L. White, S. Rocchi and two anonymous reviewers are kindly acknowledged for their constructive revision of the manuscript.

References

Armienti P, Tripodo A (1991) Petrography and chemistry of lavas and comagmatic xenoliths of Mt. Rittmann, a volcano discovered during the IV Italian expedition in Northern Victoria Land (Antarctica). Mem Soc Geol Ital 46:427–451

Armstrong RL (1978) K-Ar dating: late Cenozoic McMurdo volcanic group and Dry Valley glacial history, Victoria Land, Antarctica. N Z J Geol Geophys 21:685–698. doi:10.1080/00288306.1978.10425199

Basile I, Petit JR, Touron S, Grousset FE, Barkov N (2001) Volcanic layers in Antarctic (Vostok) ice cores: source identification and atmospheric implications. J Geophys Res Atmos 106(D23):31915–31931. doi:10.1029/2000JD000102

Behrendt JC (2012) The aeromagnetic method as a tool to identify Cenozoic magmatism in the West Antarctic Rift System beneath the West Antarctic Ice Sheet—a review; Thiel subglacial volcano as possible source of the ash layer in the WAISCORE. Tectonophysics 585:124–136. doi:10.1016/j.tecto.2012.06.035

Bonaccorso A, Mione M, Pertusati PC, Privitera E, Ricci CA (1991) Fumarolic activity at Mt. Rittmann volcano (Northern Victoria Land, Antarctica). Mem Soc Geol Ital 46:453–456

Buettner R, Dellino P, Zimanowski B (1999) Identifying modes of magma fragmentation from the surface features of ash particles. Nature 401:688–690. doi:10.1038/44364

Carey S, Bursik M (2000) Volcanic plumes. In: Sigurdsson H, Houghton BF, McNutt S, Rhymer H, Stix J (eds) Encyclopedia of volcanoes. Academic, San Diego, pp 527–554

Carey S, Sigurdsson H (1978) Deep-sea evidence for distribution of tephra from the mixed magma eruption of the Soufrière on St. Vincent, 1902: ash turbidites and air fall. Geology 6:271. doi:10.1130/0091-7613(1978)6<271:DEFDOT>2.0.CO;2

Cashman KV, Sturtevant B, Papale P, Navon O (2000) Magmatic fragmentation. In: Sigurdsson H, Houghton BF, McNutt S, Rhymer H, Stix J (eds) Encyclopedia of volcanoes. Academic, San Diego, pp 419–430

Colizza E, Finocchiaro F, Marinoni L, Menegazzo Vitturi L, Brambati A (2003) Tephra evidence in Marine Sediments from the shelf of the Western Ross Sea. Terra Antart Rep 8:121–126

Connolley WM, King JC (1993) Atmospheric water-vapour transport to Antarctica inferred from radiosonde data. Q J R Meteorol Soc 119:325–342

Curzio P, Folco L, Laurenzi MA, Mellini M, Zeoli A (2008) A tephra chronostratigraphic framework for the Frontier Mountain blue-ice field (northern Victoria Land, Antarctica). Quat Sci Rev 27:602–620. doi:10.1016/j.quascirev.2007.11.017

Davies SM, Wastegård S, Abbott PM, Barbante C, Bigler M, Johnsen SJ, Rasmussen TL, Steffensen JP, Svensson A (2010) Tracing volcanic events in the NGRIP ice-core and synchronising North Atlantic marine records during the last glacial period. Earth Planet Sci Lett 294:69–79. doi:10.1016/j.epsl.2010.03.004

Delmonte B, Basile-Doelsch I, Petit JR, Maggi V, Revel-Rolland M, Michand A, Jagoutz E, Grousset F (2004) Comparing the Epica and Vostok dust records during the last 220,000 years: stratigraphical correlation and provenance in glacial periods. Earth Sci Rev 66:63–87. doi:10.1016/j.earscirev.2003.10.004

Delmonte B, Andersson PS, Hansson M, Schöberg H, Petit JR, Basile-Doelsch I, Maggi V (2008) Aeolian dust in East Antarctica (EPICA-Dome C and Vostok): Provenance during glacial ages over the last 800 kyr.Geophys Res Lett 35. doi:10.1029/2008GL033382

Di Roberto A, Del Carlo P, Rocchi S, Panter KS (2012) Early Miocene volcanic activity and paleoenvironmental conditions recorded in tephra layers of the AND-2A core (southern MCMurdo Sound, Antarctica). Geosphere 8:1342–1355. doi:10.1130/GES00754.1

Di Vincenzo G, Skála R (2009) ^{40}Ar–^{39}Ar laser dating of tektites from the Cheb Basin (Czech republic): evidence for coevality with moldavites and influence of the dating standard on the age of the Ries impact. Geochim Cosmochim Acta 73:493–513. doi:10.1016/j.gca.2008.10.002

Di Vincenzo G, Bracciali L, Del Carlo P, Panter K, Rocchi S (2010) 40Ar–39Ar dating of volcanogenic products from the AND-2A core (ANDRILL Southern McMurdo Sound Project, Antarctica): correlations with the Erebus Volcanic Province and implications for the age model of the core. Bull Volcanol 72:487–505. doi:10.1007/s00445-009-0337-z

Dunbar NW (2002) Tephra in Siple and Taylor Dome Ice Cores. Boulder Colo USA Natl Snow Ice Data Cent. doi:10.7265/N50P0WXF

Dunbar NW (2003) Blue Ice Tephra II—Brimstone Peak. Boulder Colo USA Natl Snow Ice Data Cent. doi:10.7265/N5MG7MDK

Dunbar NW, Kurbatov AV (2011) Tephrochronology of the Siple Dome ice core, West Antarctica: correlations and sources. Quat Sci Rev 30(13–14):1602–1614. doi:10.1016/j.quascirev.2011.03.015. http://nsidc.org/data/nsidc-0110.html

Dunbar NW, Zielinski GA, Voisins DT (2003) Tephra layers in the Siple Dome and Taylor Dome ice cores, Antarctica: sources and correlations. J Geophys Res 108:2374. doi:10.1029/2002JB002056

Engwell SL, Sparks RSJ, Carey S (2014) Physical characteristics of tephra layers in the deep realm: the Campanian Ignimbrite eruption. In: Austin WEN, Abbott PM, Davies SM, Pearce NJG, Wastegård S (eds) Marine Tephrochronology, Geological Society. Special Publications, London. doi:10.1144/SP398.7, 398

Esser R, Kyle PR (2002) $^{40}Ar/^{39}Ar$ chronology the McMurdo Volcanic Group at the Pleiades, northern Victoria Land, Antarctica. Proc R Soc N Z Bull 35:415–418

Esser RP, Kyle PR, McIntosh WC (2004) $^{40}Ar/^{39}Ar$ dating of the eruptive history of Mount Erebus, Antarctica: volcano evolution. Bull Volcanol 66:671–686. doi:10.1007/s00445-004-0354-x

Fisher RV, Schmincke HU (1984) Pyroclastic rocks. Springer, Berlin

Fraser CI, Terauds A, Smellie J, Convey P, Chown SL (2014) Geothermal activity helps life survive glacial cycles. PNAS 111:5634–5639. doi:10.1073/pnas.1321437111

Froggatt PC (1992) Standardization of the chemical analysis of tephra deposits, report of the ICCT working group. Quat Int 13(14):93–96. doi:10.1016/1040-6182(92)90014-S

Fujii Y, Kohno M, Motoyama H, Matoba S, Watanabe O, Fujita S, Azuma N, Kikuchi T, Fukuoka T (1999) Ann Glaciol 29:126–130. doi:10.3189/172756499781821003

Giordano G, Lucci F, Phillips D, Cozzupoli D, Runci V (2012) Stratigraphy, geochronology and evolution of the Mt. Melbourne volcanic field (North Victoria Land, Antarctica). Bull Volcanol 74:1985–2005. doi:10.1007/s00445-012-0643-8

Harpel CJ, Kyle PR, Esser RP, McIntosh WC, Caldwell DA (2004) $^{40}Ar/^{39}Ar$ dating of the eruptive history of Mt. Erebus, Antarctica: summit flows, tephra, and caldera collapse. Bull Volcanol 66:687–702. doi:10.1007/s00445-004-0349-7

Harpel CJ, Kyle PR, Dunbar NW (2008) Englacial tephrostratigraphy of Erebus volcano, Antarctica. J Volcanol Geotherm Res 177:549–568. doi:10.1016/j.jvolgeores.2008.06.001

Heiken GH, Wholetz KH (1985) Volcanic ash. University of California Press, Berkeley, pp 1–245

Inman DL (1952) Measures for describing the size distribution of sediments. J Sediment Petrol 22(3):125–145. doi:10.1306/D42694DB-2B26-11D7-8648000102C1865D

Keys JR, Anderton PW, Kyle PR (1977) Tephra and debris layers in the Skelton Neve and Kempe Glacier, South Victoria Land, Antarctica. N Z J Geol Geophys 20(5):971–1002. doi:10.1080/00288306.1977.10420692

Kohno M, Fujii Y, Hirata T (2004) Chemical composition of volcanic glasses in visible tephra layers found in a 2503 m deep ice core from Dome Fuji, Antarctica. Ann Glaciol 39:576–584. doi:10.3189/172756404781813934

Kraus S, Kurbatov A, Yates M (2013) Geochemical signatures of tephras from Quaternary Antarctic Peninsula volcanoes. Andean Geol 40:1–40. doi:10.5027/andgeoV40n1-a01

Kyle PR (1982) Volcanic geology of the Pleiades, Northern Victoria Land, Antarctica. In: Craddock C (ed) Antarctic Geoscience. The University of Wisconsin Press, Madison, pp 747–754

Kyle PR (1990) McMurdo Volcanic Group, Western Ross Embayment. In: LeMasurier WE, Thmson JW (eds) Volcanoes of the Antarctic Plate and Southern Oceans. Am Geophys Union, Antarct Res Series 48:19–145

Kyle PR, Moore JA, Thirwall MF (1992) Petrologic evolution of anorthoclase phonolite lavas at Mt. Erebus, Ross Island, Antarctica. J Petrol 33:849–875. doi:10.1093/petrology/33.4.849

Laurenzi MA, Mellini M, Perchiazzi N (2003) $^{40}Ar/^{39}Ar$ dating of Tephra in blue ice (Northern Victoria Land, Antarctica): prospects and limitations. Terra Antart Rep 8:193–196

Le Bas MJ, Le Maitre RW, Streckeisen A, Zanettin BA (1986) Chemical classification of volcanic rocks based on the total alkali-silica diagram. J Petrol 27:745–750. doi:10.1093/petrology/27.3.745

LeMasurier WE, Thomson JW (1990) Volcanoes of the Antarctic Plate and Southern Oceans. Antarctic Research Series 48, American Geophysical Union, Washington, DC 487

Licht KJ, Dunbar NW, Andrews JT, Jennings AE (1999) Distinguishing subglacial till and glacial marine diamictons in the western Ross Sea, Antarctica: implications for a last glacial maximum grounding line. Geol Soc Am Bull 111(1):91–103. doi:10.1130/0016-7606

Lough AC, Wiens D, Barscheck CG, Anandakrishnan S, Aster RC, Blankenship DD, Huerta AD, Nyblade A, Young DA, Wilson T (2013) Seismic detection of an active subglacial magmatic complex in Marie Byrd Land, Antarctica. Nat Geosci 6:1031–1035. doi:10.1038/ngeo1992

Lowe DJ (2011) Tephrochronology and its application: a review. Quat Geochronol 6:107–153. doi:10.1016/j.quageo.2010.08.003

McPhie J, Doyle M, Allen RL (1993) Volcanic textures: A guide to the interpretation of textures in volcanic rocks: University of Tasmania, Centre for Ore Deposit and Exploration Studies

Narcisi B, Petit JR, Delmonte B, Basile-Doelsch I, Maggi V (2005) Characteristics and sources of tephra layers in the EPICA-Dome C ice record (East Antarctica): implications for past atmospheric circulation and ice core stratigraphic correlations. Earth Planet Sci Lett 239(3–4):253–265. doi:10.1016/j.epsl.2005.09.005

Narcisi B, Proposito M, Frezzotti M (2001) Ice record of a 13th century explosive volcanic eruption in northern Victoria Land, East Antarctica. Ant Sci 13(2): 174-181. doi:10.1017/S0954102001000268

Narcisi B, Petit JR, Tiepolo M (2006) A volcanic marker (92 ka) for dating deep east Antarctic ice cores. Quat Sci Rev 25(21–22):2682–2687. doi:10.1016/j.quascirev.2006.07.009

Narcisi B, Petit JR, Delmonte B (2010a) Extended East Antarctic ice-core tephrostratigraphy. Quat Sci Rev 29(1–2):21–27. doi:10.1016/j.quascirev.2009.07.009

Narcisi B, Petit JR, Chappellaz J (2010b) A 70 ka record of explosive eruptions from the TALDICE ice core (Talos Dome, East Antarctic plateau). J Quat Sci 25:844–849. doi:10.1002/jqs.1427

Narcisi B, Petit JR, Delmonte B, Scarchilli C, Stenni B (2012) A 16,000-yr tephra framework for the Antarctic ice sheet: a contribution from

the new Talos Dome core. Quat Sci Rev 49:52–63. doi:10.1016/j.quascirev.2012.06.011

Perchiazzi N, Folco L, Mellini M (1999) Volcanic ash bands in the Frontier Mountain and Lichen Hills blue-ice fields, northern Victoria Land. Antarct Sci 11(3):353–361. doi:10.1017/S0954102099000449

Renne PR, Swisher CC, Deino AL, Karner DB, Owens TL, DePaolo DJ (1998) Intercalibrations of standards, absolute ages and uncertainties in $^{40}Ar/^{39}Ar$ dating. Chem Geol 145:117–152. doi:10.1016/S0009-2541(97)00159-9

Renne PR, Mundil R, Balco G, Min K, Ludwig KR (2010) Joint determination of ^{40}K decay constants and $^{40}Ar/^{40}K$ for the Fish Canyon sanidine standard, and improved accuracy for $^{40}Ar/^{39}Ar$ geochronology. Geochim Cosmochim Acta 74:5349–5367. doi:10.1016/j.gca.2010.06.017

Sarna-Wojcicki AM, Bowman HR, Meyer CE, Russell PC, Woodward MJ, McCoy G, Rowe JJ Jr, Baedecker PA, Asaro F, Michael H (1984) Chemical analyses, correlations, and ages of upper Pliocene and Pleistocene ash layers of east-central and Southern California. USGS Professional Paper 1293

Schneider JL, Le Ruyet A, Chanier F, Buret C, Ferrière J, Proust JN, Rosseel JB (2001) Primary or secondary distal volcaniclastic turbidites: how to make the distinction? An example from the Miocene of New Zealand (Mahia Peninsula, North Island). Sediment Geol 145(1):1–22. doi:10.1016/S0037-0738(01)00108-7

Shipp S, Anderson JB, Domack EW (1999) Late Pleistocene-Holocene retreat of the West Antarctic ice-sheet system in the Ross Sea; Part 1. Geophysical results. Geol Soc of Am Bull 111:1468–1516

Smellie JL (1999) The upper Cenozoic tephra record in the south polar region: a review. Glob Planet Chang 21:51–70. doi:10.1016/S0921-8181(99)00007-7

Steiger RH, Jäger E (1977) Subcommission on geochronology: convention on the use of decay constants in geo- and cosmo- chronology. Earth Planet Sci Lett 36:359–362. doi:10.1016/0012-821X(77)90060-7

Stern C (1990) Tephrochronology of southernmost Patagonia. Natl Geogr Res 6:110–126

Stern C (2008) Holocene tephrochronology record of large explosive eruptions in the southernmost Patagonian Andes. Bull Volcanol 70:435–454. doi:10.1007/s00445-007-0148-z

Wilch TI, McIntosh WC, Dunbar NW (1999) Late Quaternary volcanic activity in Marie Byrd Land: potential $^{40}Ar/^{39}Ar$-dated time horizons in West Antarctic ice and marine cores. Geol Soc Am Bull 111(10):1563–1580